Experimental Hematology

Experimental Hematology 2019;70:70–84

Smc3 is required for mouse embryonic and adult hematopoiesis

Tianjiao Wang[a], Brandi Glover[a], Gayla Hadwiger[a], Christopher A. Miller[a,b], Orsola di Martino[a], and John S. Welch[a]

[a]*Department of Internal Medicine, Washington University School of Medicine, St. Louis, MO, USA;* [b]*McDonnell Genome Institute, Washington University School of Medicine, St. Louis, MO, USA*

(Received 20 November 2018; accepted 28 November 2018)

SMC3 **encodes a subunit of the cohesin complex that has canonical roles in regulating sister chromatids segregation during mitosis and meiosis. Recurrent heterozygous mutations in *SMC3* have been reported in acute myeloid leukemia (AML) and other myeloid malignancies. In this study, we investigated whether the missense mutations in *SMC3* might have dominant-negative effects or phenocopy loss-of-function effects by comparing the consequences of *Smc3*-deficient and -haploinsufficient mouse models. We found that homozygous deletion of *Smc3* during embryogenesis or in adult mice led to hematopoietic failure, suggesting that *SMC3* missense mutations are unlikely to be associated with simple dominant-negative phenotypes. In contrast, haploinsufficiency was tolerated during embryonic and adult hematopoiesis. Under steady-state conditions, *Smc3* haploinsufficiency did not alter colony forming in methylcellulose, only modestly decreased mature myeloid cell populations, and led to limited expression changes and chromatin alteration in $Lin^{-}cKit^{+}$ bone marrow cells. However, following transplantation, engraftment, and subsequent deletion, we observed a hematopoietic competitive disadvantage across myeloid and lymphoid lineages and within the stem/progenitor compartments. This disadvantage was not affected by hematopoietic stresses, but was partially abrogated by concurrent *Dnmt3a* haploinsufficiency, suggesting that antecedent mutations may be required to optimize the leukemogenic potential of *Smc3* mutations. Published by Elsevier Inc. on behalf of ISEH – Society for Hematology and Stem Cells.**

Acute myeloid leukemia (AML) is an aggressive hematopoietic malignancy characterized by the accumulation of myeloblasts in the blood or bone marrow (BM) with maturation arrest and retained self-renewal [1]. Tremendous progress has been made in identifying recurrent gene mutations in AML, yet we are still in the early stages of understanding the mechanisms through which these genetic alterations contribute to the onset of the disease [2].

Recurring mutations in the cohesin complex occur in four core components: *SMC3, SMC1A, RAD21*, and *STAG2*, and have been identified in AML and other myeloid malignancies [3–5]. More than 50% of patients with Down syndrome-associated acute megakaryocytic leukemia have cohesin mutations, specifically in *STAG2* [6]. Somatic cohesin mutations have also been observed in a variety of solid cancers, including colorectal carcinoma, ovarian carcinoma, glioblastoma, bladder carcinoma, and Ewing's sarcoma [7–12]. Additionally, germline mutations of the cohesin complex are causally related to developmental disorders, particularly cohesinopathies such as Cornelia de Lange syndrome [13,14].

SMC3 and *RAD21* mutations are nearly universally heterozygous, whereas mutations in *SMC1A* and *STAG2* may be hemizygous because they are X-linked. Cohesin mutations also tend to be mutually exclusive, implying that alteration in one component may be sufficient to disrupt the entire complex or alternatively, they may not be tolerated by a cell when co-occurring [15,16]. Cohesin mutations are often observed as early subclonal events in AML, conceivably facilitating disease initiation, although they are not observed in cases of clonal hematopoiesis of indeterminate potential (CHIP), suggesting they are unlikely to be the initiating event [15,17–19].

Offprint requests to: John S. Welch, MD, PhD, Division of Oncology, Department of Internal Medicine, Washington University School of Medicine, 660 South Euclid Ave., Box 8007, St. Louis, MO 63110; E-mail: jwelch@wustl.edu

Supplementary material associated with this article can be found, in the online version, at doi:10.1016/j.exphem.2018.11.008.

0301-472X/Published by Elsevier Inc. on behalf of ISEH – Society for Hematology and Stem Cells.
https://doi.org/10.1016/j.exphem.2018.11.008

The majority of *SMC3* mutations are missense mutations; only one-third of *SMC3* mutations are nonsense or splice-site variants. The missense mutations are scattered across all domains, although a few recurrently mutated nucleotides have been observed (e.g., R381Q, R661P). This pattern suggests that many of these mutations may result in simple loss-of-function consequences, although novel dominant-negative activities cannot be dismissed within the hotspot variants. Intriguingly, *DNMT3A* mutations, one of the most commonly mutated genes in AML, frequently coincides with *SMC3* mutations, suggesting there may be leukemogenic interactions between these mutations [5,15,16,20].

In yeast- and cell-line-based studies, cohesin has been shown to play essential roles in sister chromatid segregation during the cell cycle, DNA damage repair, transcriptional regulation via chromatin looping, and maintenance of chromatin architecture [21–24]. AML patients who harbor cohesin mutations typically have normal karyotype, indicating that hematopoietic cohesin mutations do not lead directly to chromosomal instability [3,16].

To define the hematopoietic consequences of *SMC3* mutations and to determine whether these could reflect dominant-negative or loss-of-function phenotypes, we characterized the in vivo effects of *Smc3* deficiency and *Smc3* haploinsufficiency on murine hematopoiesis using conditionally deleted strategies. In contrast to our expectations that these leukemia-associated mutations would lead to expansions of hematopoietic stem cell populations or augmented self-renewal, we observed a competitive disadvantage in *Smc3*-deficient and -haploinsufficient BM cells in vivo without an associated increase in maturation-arrested stem cells.

Methods

Animal Studies

Smc3^{trap} mice were obtained from the European Conditional Mouse Mutagenesis Program (EUCOMM) (Smc3<tm1a (EUCOMM)Wtsi>, MGI:4434007). To generate *Smc3*^{fl} mice, the gene-trap was removed by crossing *Smc3*^{trap} mice with Flp deleter mice (B6.129S4-Gt(ROSA)26Sortm2(FLP*)Sor/J) and subsequently outbreeding the Flp allele with C57BL/6J intercrosses. We generated *Smc3* conditional-deficient mice by breeding the *Smc3*$^{fl/fl}$ mice with *Vav1-Cre* (B6.Cg-Commd10Tg(Vav1-icre)A2Kio/J), *ERT2-Cre* (B6.Cg-Tg(cre/Esr1)5Amc/J), and *CMV-Cre* (B6.C-Tg(CMV-cre)1Cgn/J) mice obtained from The Jackson Laboratory. We characterized *Smc3* conditional-deficient mice at 6–8 weeks of age and both genders were used. Whenever possible, littermate controls were used for all experiments. Complete blood counts were measured using Hemavet 950 (Drew Scientific Group).

All mice were on the C57BL/6 background and were cared for in the Experimental Animal Center of Washington University School of Medicine. The Washington University Animal Studies Committee approved all animal experiments.

Intracellular Smc3 staining

Intracellular Smc3 was detected with the Pharmingen Transcription Factor Buffer Set (BD Biosciences, #562574) according to the manufacturer's instructions. BM cells were isolated from femurs and tibias and lysed with ACK lysis buffer (150 mmol/L NH_4Cl, 10 mmol/L $KHCO_3$, and 0.1 mmol/L Na_2EDTA [Na_2-ethylenediaminetetraacetic acid], pH 7.2–7.4). Cells were stained with cell-surface markers to identify cell type by flow cytometry and then fixed for 40 minutes at 4°C. Cells were washed with permeabilization wash buffer and incubated with primary antibody against Smc3 (1:100 dilution, Abcam, #ab9263) for 30 minutes at 4°C. Cells were washed in permeabilization wash buffer and incubated in secondary antibody (1:500 dilution, chicken anti-rabbit Alexa Fluor 647, Molecular Probes) for 30 minutes at 4°C. Cells were rinsed in permeabilization wash buffer and analyzed by flow cytometry. The mean fluorescence intensity was calculated for the AF647 signal.

Flow cytometry

After lysis of red blood cells by ACK lysis buffer, peripheral blood, BM, spleen cells, or thymocytes were treated with anti-mouse CD16/32 (eBioscience; clone 93) and stained with the indicated combinations of the following antibodies (all antibodies are from eBioscience unless noted otherwise): CD34 FITC (clone RAM34), CD11b PE (clone M1/70), c-Kit PECy7 (clone 2B8) or BV421 (BioLegend, clone 2B8), Sca1 PE-Dazzle 594 (BioLegend, clone D7) or APC (clone D7), Gr-1 FITC, PECy7, APC (clone RB6-8C5), or BV421 (BioLegend, clone RB6-8C5), B220 PE, PECy7, APC (clone RA3-6B2), or APC-Cy7 (BioLegend, clone RA3-6B2), CD3 PECy7 (clone 145-2C11), CD71 PE(clone R17217), Ter-119 PECy7 or APC (clone TER-119), CD16/32 BV510 (clone 93), CD150 PE (BioLegend 115903, clone TC15-12F12.2), CD48 APC-Cy7 (BioLegend, clone HM48-1), Ly5.1 APC (clone A20) or AF700 (BioLegend, clone A20), Ly 5.2 PE or e450 (clone 104). The following flow phenotypes were used for stem and progenitor cell flow: Lin- (lineage negative): $B220^-$, $CD3e^-$, $Gr\text{-}1^-$, $Ter\text{-}119^-$, $CD4^-$, $CD8^-$, $CD19^-$, $CD127^-$; KL: Lin^-, $cKit^+$, $Sca1^-$; KLS: Lin^-, $cKit^+$, $Sca\text{-}1^+$; KLS-SLAM: Lin^-, $cKit^+$, $Sca\text{-}1^+$, $CD150^+$, $CD48^-$; GMP: Lin^-, $cKit^+$, $Sca\text{-}1^-$, $CD34^+$, $CD16/32^+$; CMP: Lin^-, $cKit^+$, $Sca\text{-}1^-$, $CD34^+$, $CD16/32^-$; and MEP: Lin^-, $cKit^+$, $Sca\text{-}1^-$, $CD34^-$, $CD16/32^-$-.

Analysis was performed using a FACScan (Beckman Coulter) or Gallios flow cytometer (Beckman Coulter). Cell sorting was performed using a I-Cyt Synergy II sorter (I-Cyt Technologies). Flow cytometry data were analyzed with FlowJo Version 10 (TreeStar), Excel (Microsoft), and Prism 7.02 (GraphPad Software) software.

Competitive transplantation

Competitive transplantation was performed using 0.5×10^6 whole BM cells from indicated donor mice (CD45.2) mixed with 0.5×10^6 competitor whole BM cells wild-type CD45.1 (Ly5.1) × CD45.2 mice. Mixture cells were injected intravenously into 6- to 8-week-old CD45.1 recipient mice that received 1100 cGy of total body irradiation (Mark 1 Cesum irradiator, J.L. Shepard) 24 hours prior to

transplantation. For *Smc3*$^{fl/fl}$*/ERT2-Cre*$^{+/-}$ or *Smc3*$^{fl/+}$*/ERT2-Cre*$^{+/-}$ transplantation, recipient mice were treated with tamoxifen (TAM) (dissolved in sterile corn oil, Sigma-Aldrich) 6 weeks after transplantation via oral gavage for nine doses (3 mg/day/mouse, 3 days/week). Peripheral blood was examined for donor cell chimerism at the indicated time points after transplantation. Recipient mice BM were analyzed at the end of the experiment.

Colony replating assay

BM cells were harvested and plated in duplicate (10,000 BM cells/plate) in complete mouse methylcellulose medium with stem cell factor, interleukin-3 (IL-3), IL-6, and erythropoietin (Epo) (R&D Systems). Colonies were counted on day 7 and cells were collected from methylcellulose in warm Dulbecco-modified Eagle medium (DMEM) containing 2% fetal bovine serum, washed, and replated as before. An aliquot of cells was taken for analysis of myeloid (Gr1, CD11b) and mast cell markers (cKit, FcER1) by flow cytometry. This process was repeated for 4 weeks or until colony formation failed.

RNA sequencing of multipotent progenitors and analysis

Multipotent progenitors (KLs) were sorted from three wild-type or *Smc3*$^{fl/+}$*/Vav1-Cre*$^{+/-}$ mice into DMEM. Flow cytometry of samples after sorting validated >93% sort accuracy. RNA was extracted from cell pellets using a miRNeasy kit (QIAGEN) and genomic DNA was removed by the RNase-Free DNase Set (QIAGEN). RNA was analyzed for degradation using the RNA Nano Chip (Agilent Technologies, #5067-1521). An input of 300 ng was taken forward for each sample using the TruSeq Stranded Total RNA with Ribo-Zero Globin Kit (Illumina, #20020612). Final libraries were analyzed using a high-sensitivity DNA chip (Agilent Technologies, #5067-4626). All libraries were pooled and run across three lanes of HiSeq4000. RNAseq data were aligned to the human reference with Tophat version 2.0.8 (denovo mode, params: −library-type fr-firststrand −bowtie-version = 2.1.0). Expression levels were calculated with Cufflinks version 2.1.1 (params: −max-bundle-length 10000000 −max-bundle-frags 10000000) [25].

Assay for transposase-accessible chromatin sequencing of multipotent progenitor and analysis

Chromatin accessibility assays using the bacterial Tn5 transposase were performed using multipotent progenitors (KLs) sorted from *Smc3*$^{fl/+}$ or *Smc3*$^{fl/+}$*/Vav1-Cre*$^{+/-}$ mice in triplicate. DNA was prepared from 75,000 sorted cells and >93% sorting accuracy verified with post-sort analysis. Assay for transposase-accessible chromatin (ATAC) libraries were generated exactly as described previously [26] and pooled and sequenced on a HiSeqX instrument (Illumina) to obtain between 133 and 152 million 2 × 150 bp paired-end reads. Raw sequencing reads were adapter trimmed with trim galore using cutadapt version 1.8.1 (Martin EMBnet 2011) and then aligned to the mouse reference genome (mm10) using bwa mem (Li H. arXiv:1303.3997v1 (2013)). Peaks in each sample were identified with macs2 [27] using the -f BAMPE parameter and then filtered to retain peaks with $q < 0.01$. Peak summits from all samples were merged together with BEDtools merge [28] using parameters to combine summits within 50 bp of each other. Read counts at the merged peak summits were obtained for all samples using the deepTools multiBamSummary command [29] with the minimum mapping quality set to 1 and then processed using DESeq2 [30] with default parameters to obtain normalized counts for each peak summit and to perform differential analysis across all peaks between wild-type and mutant mice.

Statistics

Statistical analysis was performed using Prism version 7.02 (GraphPad Software) and Excel (Microsoft) software. Unpaired two-tailed *t* test and one-way and two-way ANOVA with Tukey's multiple-comparisons tests were performed as appropriate. p values < 0.05 were considered statistically significant. Error bars represent standard deviation (SD). Data points without error bars have SD below Prism 7.02's limit to display.

Results

Generation of Smc3 conditional knockout mice

To investigate the effects of *Smc3* loss on hematopoiesis, we generated *Smc3* conditionally deficient and haploinsufficient mice using Smc3<tm1a(EUCOMM)Wtsi> mice obtained from EUCOMM (*Smc3*^{trap}). The *Smc3*^{trap} allele has a lacZ-neomycin-gene-trap cassette inserted in intron 4 with two Frt sites on each side of the cassette and two loxP sites flanking exon 4. The gene trap is predicted to lead to an early transcription stop after splicing into lacZ-neomycin. The conditional knockout *Smc3*^{fl} allele was created by excising the gene-trap cassette with Flp recombinase and was used for further characterizations because homozygous deletion could be achieved using the *Smc3*^{fl} allele (Figure 1A). We validated the integration of the loxP sites surrounding exon 4 in the *Smc3*^{fl} allele using whole-genome sequencing (Figure 1B).

We examined the transcriptional consequences of the *Smc3*^{fl} allele using RNA sequencing (RNA-Seq) and intracellular flow cytometry. In BM cells from three *Smc3*$^{fl/+}$*/Vav1-Cre*$^{+/-}$ mice, nearly 50% (48.4%) of transcripts spliced from exons 3 to 5, consistent with deletion of exon 4, whereas all of the wild-type transcripts spliced from exons 3 to 4 and exons 4 to 5 (Figure 1C and Supplementary Figure E1A-F). Analysis of reads spanning exons 3 to 5 suggests that this results in a frameshift mutation and a stop codon after 59 amino acids, although this truncated protein could not be detected using N-terminal antibodies. Using C-terminal antibodies, the intracellular Smc3 protein level was reduced to approximately half of littermate control, as would be expected with a heterozygous allele and confirming *Smc3* haploinsufficiency (Figure 1D). In addition, the Smc3 protein level was regulated during normal hematopoiesis, with higher expression in

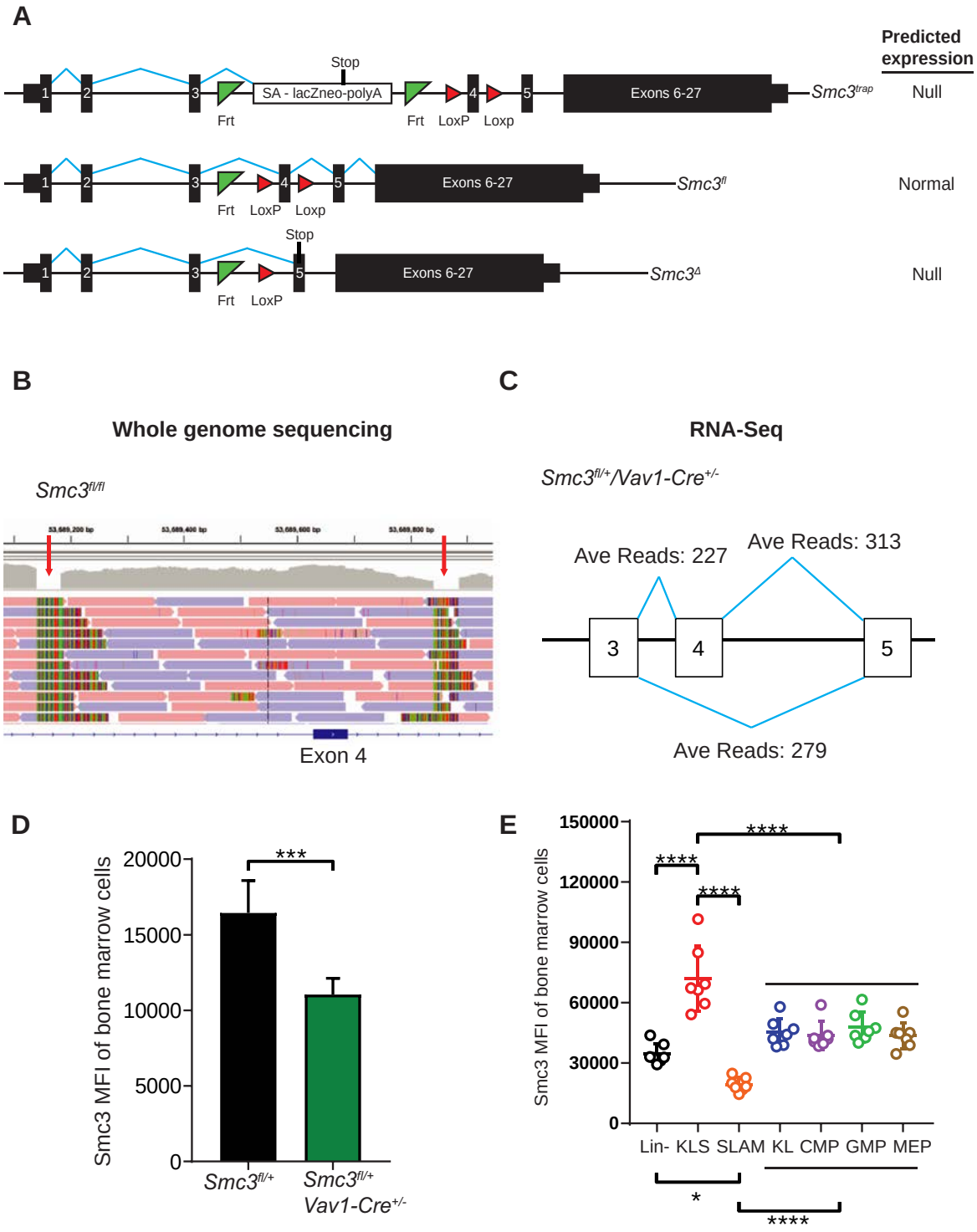

Figure 1. Generation of *Smc3* conditional deficient mice and allele validation. **(A)** The *Smc3*-haploinsufficient mouse model ($Smc3^{trap/+}$) was obtained from EUCOMM. *Smc3* conditional-deficient mice were generated by removing the gene-trap cassette, which retains the loxP sites flanking exon 4 ($Smc3^{fl/+}$) and crossing these mice with either $Vav1\text{-}Cre^{+/-}$ or $ERT2\text{-}Cre^{+/-}$ to delete the allele ($Smc3^{\Delta/+}$). All mice are on the C57BL/6J background. **(B)** Whole-genome sequencing validation of $Smc3^{fl}$ integration sites. **(C)** RNA-Seq data of the $Smc3^{fl/+}/Vav1\text{-}Cre^{+/-}$ mice showing 227 transcripts spliced from exons 3 to 4 and then 313 transcripts from exons 4 to 5, whereas 279 transcripts from the other allele spliced from exons 3 to 5 (average data from three mice). **(D)** *Smc3* haploinsufficiency was confirmed by reduced Smc3 level in the BM cells of the $Smc3^{fl/+}/Vav1\text{-}Cre^{+/-}$ mice measured using intracellular flow cytometry ($n = 5$). *Statistical significance by *t* test, ***$p < 0.001$. **(E)** Smc3 level is significantly higher in KLS cells and progenitor populations than in Lin^- and SLAM. *Statistical significance by one-way ANOVA with Tukey's multiple-comparisons test, ****$p < 0.0001$.

KLS stem/progenitor cells versus SLAM stem cells (Figure 1E). Representative primary intracellular flow data are shown in Supplementary Figure E2 (online only, available at www.exphem.org).

Homozygous Smc3 deletion

To determine whether *SMC3* mutations might have dominant-negative effects or phenocopy loss-of-function effects, we compared the consequences of *Smc3*-deficient and -haploinsufficient mouse models. We found that hematopoietic homozygous deletion of *Smc3* led to embryonic lethality. In heterozygous *Smc3*$^{fl/+}$*/Vav1-Cre*$^{+/-}$ intercrosses, we observed 0 out of 75 pups with homozygous *Smc3* alleles (Figure 2A). To determine whether the cause of death in *Smc3*$^{fl/fl}$*/Vav1-Cre*$^{+/-}$ embryos was from hematopoietic failure, we examined embryonic day 13.5 (E13.5) embryos. Grossly, the *Smc3*$^{fl/fl}$*/Vav1-Cre*$^{+/-}$ embryos were indistinguishable in size and appearance from other genotypes except for the lack of obvious fetal livers (Figures 2B and 2C). A severe decrease in fetal liver hematopoietic cells was verified by cell count and flow cytometry with near-complete absence of CD45$^+$ Gr1$^+$ CD11b$^+$ cells demonstrating myeloid-biased hematopoietic failure (Figures 2D–2F).

We investigated somatic homozygous *Smc3* deletion in adult mice using the *Smc3*$^{fl/fl}$*/ERT2-Cre*$^{+/-}$ mice. *Smc3* deletion was achieved by treating mice with oral TAM at 6 weeks of age and reduction in Smc3 protein confirmed with Western blot (Supplementary Figure EE3A, online only, available at www.exphem.org). After four doses of TAM, mice were moribund and therefore were sacrificed for analysis. Complete blood count (CBC) data showed the *Smc3*$^{fl/fl}$*/ERT2-Cre*$^{+/-}$ mice had lower white blood cell counts; percentages of lymphocytes and monocytes; and fewer platelets than TAM-treated littermates (Figure 3A). The *Smc3*$^{fl/fl}$*/ERT2-Cre*$^{+/-}$ mice had decreased spleen weights (Figure 3B) and their spleens were smaller in size (Supplementary Figure E3B, online only, available at www.exphem.org). Total numbers of cells in the BM, spleen, and thymus of the *Smc3*$^{fl/fl}$*/ERT2-Cre*$^{+/-}$ mice were significantly reduced compared with *Smc3*$^{fl/fl}$ mice after TAM treatment (Figure 3C). The reduction of cells occurred across all lineages in the BM (Figure 3D), spleen, and thymus (Supplementary Figures E3C and E3D, online only, available at www.exphem.org) of the *Smc3*$^{fl/fl}$*/ERT2-Cre*$^{+/-}$ mice, suggesting complete hematopoietic collapse.

Because activation of ERT2-Cre leads to *Smc3* deletion in a wide range of cells and tissues, we repeated these studies, isolating hematopoietic cells via a competitive transplantation. Equivalent engraftment of transgenic CD45.2$^+$ and competitor CD45.1$^+$ CD45.2$^+$ cells was verified 6 weeks after transplantation. Following TAM-induced *Smc3* deletion, the *Smc3*$^{fl/fl}$*/ERT2-Cre*$^{+/-}$ donor cells were quickly outcompeted, indicating complete loss of hematopoietic stem and progenitor cell (HSPC) functions in the *Smc3*$^{fl/fl}$*/ERT2-Cre*$^{+/-}$ BM. Once again, the effect was most pronounced within the myeloid compartment (Figures 3E and 3F), suggesting that myeloid hematopoiesis is sensitive to *Smc3* deletion, so the AML-associated *SMC3* mutations are unlikely to have simple dominant-negative effects.

Steady-state heterozygous Smc3 deletion

In the ExAC database (exac.broadinstitute.org), no *SMC3* loss-of-function mutations are observed in available human data (0 observed vs. 58.5 expected mutations), suggesting potential embryonic lethality or reduced fitness associated with *Smc3* haploinsufficiency. We therefore determined whether *Smc3* haploinsufficiency might be tolerated in mice. Because *CMV-Cre* is X-linked and expressed during early embryogenesis, we examined the ratio of male: female pups and compared difference between genders to determine whether embryonic *Smc3* haploinsufficiency altered hematopoiesis. We found that *Smc3* haploinsufficiency led to a normal number of female pups in *CMV-Cre* intercrosses (Supplementary Figure E4A, online only, available at www.exphem.org) and the female pups had no obvious defects in CBCs, total numbers of BM cells, and percentages of HSPCs and cells in different lineages (Supplementary Figures E4B–E4E, online only, available at www.exphem.org). Therefore, embryonic *Smc3* haploinsufficiency could be tolerated and did not grossly perturb steady-state hematopoiesis in mice.

We next assessed the effects of somatic *Smc3* haploinsufficiency on hematopoiesis using the inducible *Smc3*$^{fl/+}$*/ERT2-Cre*$^{+/-}$ mice. *Smc3* haploinsufficiency did not alter the proportions of immunophenotypic HSPCs and cells of different lineages (Figures 4A and 4B).

Furthermore, *Smc3* haploinsufficiency did not increase the number of colonies formed in methylcellulose or the average number of cells per colony and the *Smc3* haploinsufficient BM cells did not replate beyond 2 weeks (Figures 4C–4E). At the end of each week, the colonies on each plate were collected, washed, and characterized by immunophenotype. At the end of week 1, the cells were predominantly Gr1$^+$ CD11b$^+$ for both the *Smc3*$^{fl/+}$*/ERT2-Cre*$^{+/-}$ and *Smc3*$^{fl/+}$ genotypes. However, starting week 2, the colonies shifted to cKit$^+$ FcER1$^+$ mast cells. In weeks 3 and 4, the few colonies left were exclusively mast cells (Supplementary Figures E5A and E5B, online only, available at www.exphem.org). Similar results were observed using BM cells from *Smc3*$^{fl/+}$*/Vav1-Cre*$^{+/-}$ mice.

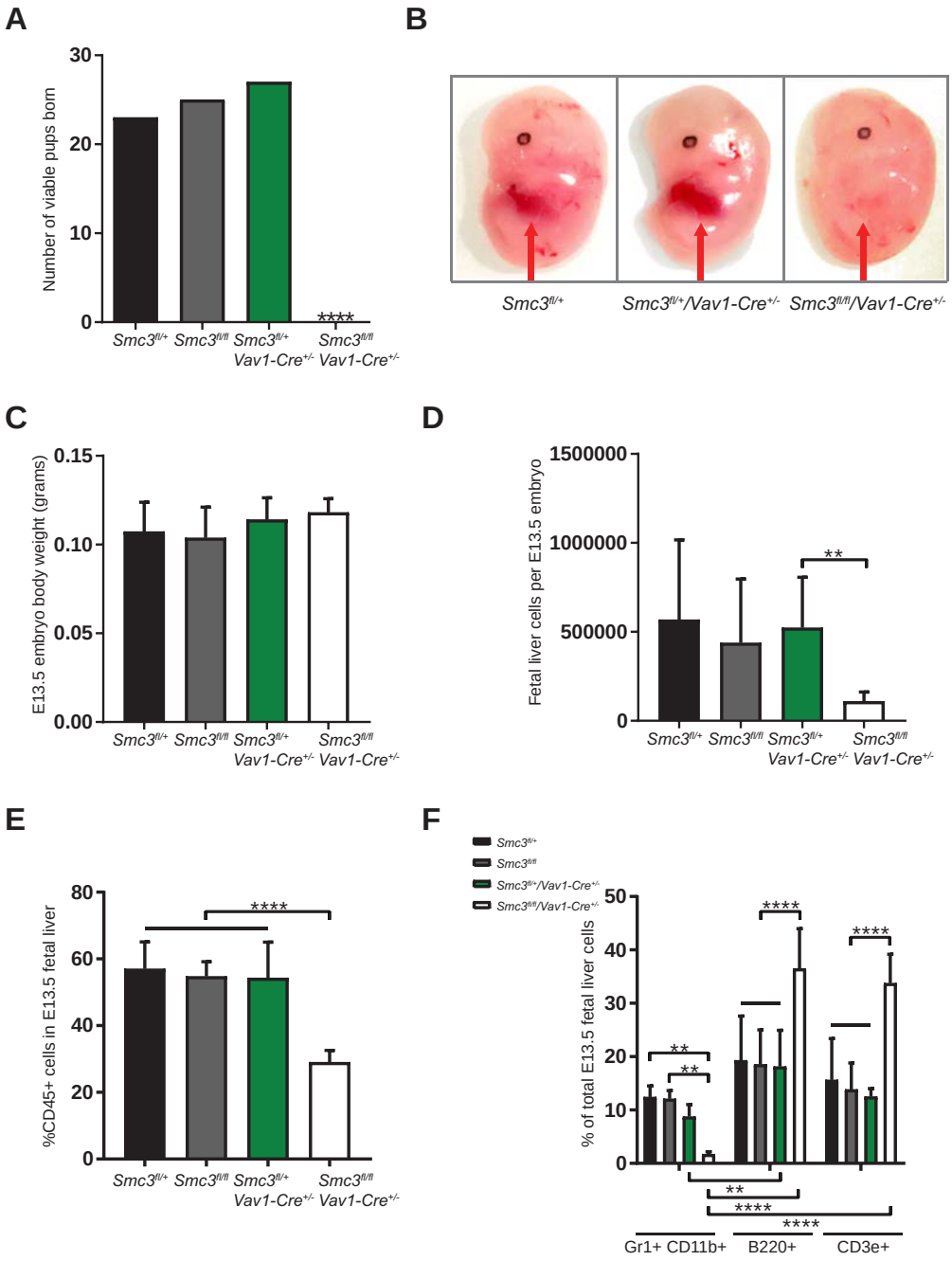

Figure 2. Embryonic hematopoietic *Smc3* deletion. **(A)** No *Smc3*$^{fl/fl}$*/Vav1-Cre*$^{+/-}$ pups were observed following *Smc3*$^{fl/+}$ and *Smc3*$^{fl/+}$*/Vav1-Cre*$^{+/-}$ intercrosses ($n = 11$ litters). *Statistical significance by chi-squared test, ****$p < 0.0001$. **(B,C)** The E13.5 *Smc3*$^{fl/fl}$*/Vav1-Cre*$^{+/-}$ embryos lacked gross fetal livers **(B)** but retained normal body weight **(C)** compared with littermates. **(D,E)** The E13.5 *Smc3*$^{fl/fl}$*/Vav1-Cre*$^{+/-}$ embryos had decreased total fetal liver cells **(D)** and fetal liver hematopoietic cells (CD45.2$^+$) **(E).** **(F)** Myeloid (Gr1$^+$CD11b$^+$) cells were reduced and increased proportions of B220$^+$ and CD3e$^+$ lymphocytes were observed in E13.5 *Smc3*$^{fl/fl}$*/Vav1-Cre*$^{+/-}$ fetal livers compared with littermate controls. **(C–F)** $n = 7$ embryos per group. *Statistical significance by one-way **(D,E)** and two-way **(F)** ANOVA with Tukey's multiple-comparisons test, **$p < 0.01$, ****$p < 0.0001$.

We performed RNA-Seq to measure global gene expression in *Smc3*-haploinsufficient hematopoietic progenitors (Lin-cKit$^+$Sca1$^-$) using the constitutive *Smc3*$^{fl/+}$*/Vav1-Cre*$^{+/-}$ model. This model was chosen because it required minimal manipulation of the mice, provided hematopoietic-restricted deletion, and would evaluate steady-state hematopoietic conditions. Multipotent progenitors (KLs) were sorted from age-matched individual wild-type and *Smc3*$^{fl/+}$*/Vav1-Cre*$^{+/}$ mice for RNA-Seq. KLs were selected because *Smc3* haploinsufficiency

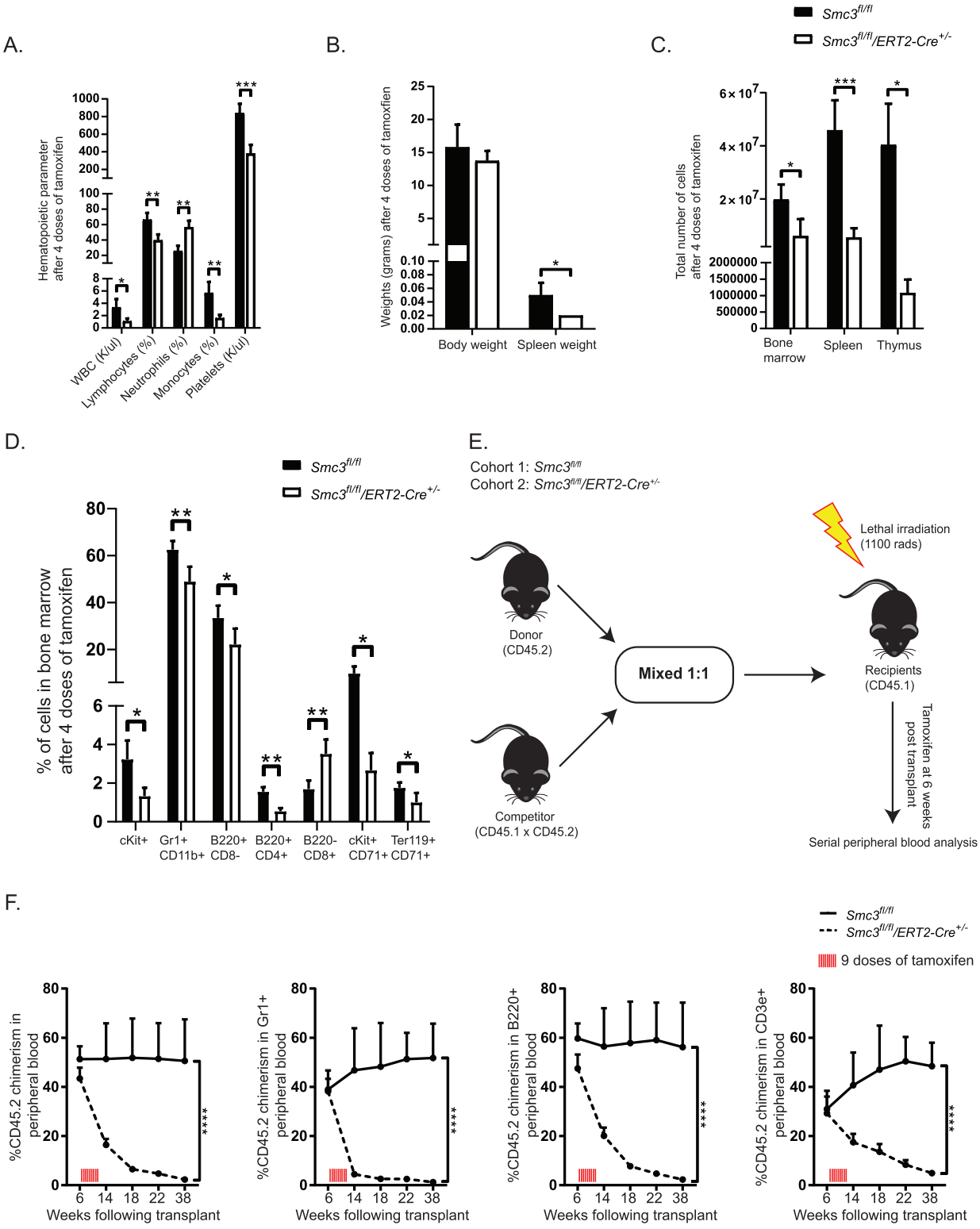

Figure 3. Homozygous somatic *Smc3* deletion. **(A)** *Smc3*$^{fl/fl}$/*ERT2-Cre*$^{+/-}$ and *Smc3*$^{fl/fl}$ littermate control mice were treated with four doses of TAM (3 mg/day orally on days 1, 3, 5, and 8 analyzed on day 8; $n = 4$ mice in each group). **(A)** Peripheral blood analysis. **(B)** Body weight and spleen weight. **(C)** Total number of cells in the BM, spleen, and thymus. **(D)** Analysis of lineage percentages within total BM cells. **(A–D)** $n = 4$ mice per group, *Statistical significance by *t* test, *$p < 0.05$, **$p < 0.01$, ***$p < 0.001$. **(E)** Experimental schema of the *Smc3*$^{fl/fl}$/*ERT2-Cre*$^{+/-}$ competitive transplantation. **(F)** Recipient mice treated with TAM after 6-week engraftment. After TAM-mediated deletion, *Smc3*-deficient cells were rapidly outcompeted, with earliest cell loss in the Gr1^{+} myeloid compartment showing as complete competitive disadvantage. *Statistical significance by two-way ANOVA with Tukey's multiple-comparisons test, ****$p < 0.0001$. **(E,F)** $n = 10$ mice per group.

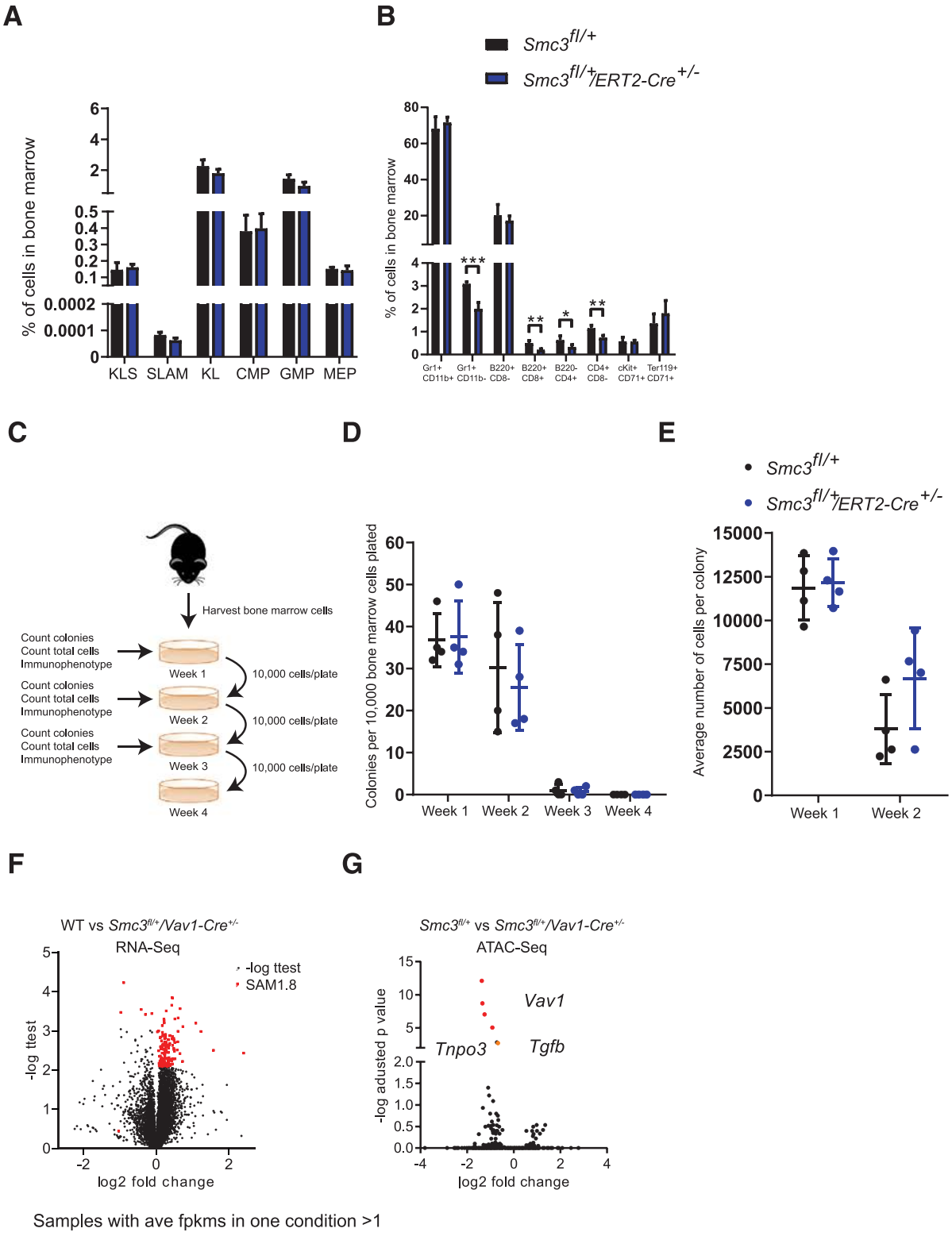

Figure 4. Steady-state *Smc3* haploinsufficiency. **(A,B)** Distribution of BMBM stem, progenitor, and lineage populations in *Smc3*$^{fl/+}$*/ERT2-Cre*$^{+/-}$ and littermate *Smc3*$^{fl/+}$ mice following nine doses of TAM ($n = 6$ mice per group). **(C)** Experimental schema of serial replating assay. **(D,E)** Colony numbers and average cells per colony on indicated week of plating in methylcellulose ($n = 4$ mice per group). *Statistical significance by *t* test, *$p < 0.05$, **$p < 0.01$, ***<0.001. **(F)** Expression analysis by RNA-Seq data of KL BM cells from *Smc3*$^{fl/+}$*/Vav1-Cre*$^{+/-}$ mice compared with wild-type cells ($n = 3$ mice per group). **(G)** Comparison of relative peak intensity identified by ATAC-Seq of KL BM cells from *Smc3*$^{fl/+}$*/Vav1-Cre*$^{+/-}$ compared with wild-type cells ($n = 3$ mice per group).

resulted in severe multilineage competitive disadvantage in vivo, suggesting potential defect in the functions of *Smc3*-haploinsufficient KLs. However, minimal global transcriptional changes were detected. Using *t* tests and significance analysis of microarrays [31], 149 genes were identified with differential expression in *Smc3*-haploinsufficient KLs compared with wild-type controls (most with less than twofold changes) (Figure 4F). KEGG pathway analysis showed significance ($p < 0.002$ and $p < 0.005$) for progesterone-mediated oocyte maturation and toxoplasmosis, respectively, but these are not related to hematopoiesis [32]. *Smc3* expression was not observed to be different when analyzed using total reads across the entire gene. However, we observed a twofold reduction in the expression of exon 4 consistent with deletion of this exon (Figure 1C).

To determine whether *Smc3* haploinsufficiency might lead to alterations in global chromatin structure that may be biologically relevant but did not lead to measurable altered gene transcription, we performed transposase-accessible chromatin sequencing (ATAC-Seq). Chromatin accessibility peaks of the *Smc3*$^{fl/+}$*/Vav1-Cre*$^{+/}$ KLs and littermate *Smc3*$^{fl/+}$controls revealed by ATAC-Seq were not significantly different except for peaks in proximity of three genes: *Vav1, Tnpo3*, and *Tgfb* (Figure 4G). The twofold difference in *Vav1* was expected for the heterozygous allele and therefore indicated the fidelity of the data generated by the assay.

Phenotypes of Smc3 haploinsufficiency following competitive transplantations

AML emerges following clonal expansion. Therefore, we conducted competitive transplantation using the inducible *ERT2-Cre* model instead of the constituent hematopoietic *Vav1-Cre* so that complete engraftment could be verified 6 weeks after transplantation prior to deletion of the *Smc3* allele. In competitive transplantations, we observed a significant competitive disadvantage in the *Smc3*$^{fl/+}$*/ERT2-Cre*$^{+/-}$ BM cells (Figure 5A). End-point analysis of BM cells also showed competitive disadvantage in the *Smc3*$^{fl/+}$*/ERT2-Cre*$^{+/-}$ HSPCs and across the myeloid, B-,and T-cell lineages, implying impaired HSPC functions due to *Smc3* haploinsufficiency in the BM and not a defect in hematopoietic peripheralization or maturation (Figures 5B–5F). The competitive disadvantage was observed first in the Gr1 myeloid compartment, perhaps due to higher turnover of these cells (Figure 5D). To verify that the competitive disadvantage observed was not due to the toxicity of ERT2-Cre, we repeated the competitive transplantation with the *ERT2-Cre*$^{+/-}$ control mice. The chimerisms of overall CD45.2^{+} cells and of CD45.2^{+} cells in all lineages were well-preserved, eliminating the possibility of ERT2-Cre toxicity (Supplementary Figures E6A and E6B, online only, available at www.exphem.org).

The absence of preleukemic delayed maturation or augmented self-renewal in *Smc3*-haploinsufficient mice was unexpected. Therefore, we determined whether *Smc3* haploinsufficiency might increase self-renewal if it occurred in combination with specific conditions of hematopoietic stress. We again observed a competitive disadvantage in the *Smc3*$^{fl/+}$*/ERT2-Cre*$^{+/-}$ BM cells following TAM induction. Intriguingly, the significant myeloid competitive disadvantage was ameliorated at 18 weeks after transplantation in the pIpC-treated group, whereas it was accelerated in the 5-fluorouracil (5-FU)-treated group, although this effect was transient and, by week 26, the donor cell populations were equivalently reduced Figure 5G-J.

Dnmt3a haploinsufficiency partially abrogated myeloid competitive disadvantage in Smc3-haploinsufficient BM cells

In AML patients, *DNMT3A* mutations co-occurred in approximately one-third of the cases with *SMC3* mutations that assess additional mutations [4,5,15,16]. We therefore investigated whether *Smc3* haploinsufficiency might lead to a competitive advantage if it occurred in the background of *Dnmt3a* haploinsufficiency [20].

We observed that with the addition of *Dnmt3a* haploinsufficiency, the severe competitive disadvantage was partially abrogated in the *Smc3*$^{fl/+}$*/ERT2-Cre*$^{+/-}$ myeloid cells, but the significant competitive disadvantage in other lineages remained intact (Figures 6A-6D). The same phenotype was observed in the *Smc3*$^{fl/+}$*/ERT2-Cre*$^{+/-}$*/Dnmt3a*$^{+/-}$ BM upon end-point analysis(Figures 6E). Accordingly, even with constitutive *Dnmt3a* haploinsufficiency, *Smc3* haploinsufficiency did not result in competitive growth advantage in hematopoietic cells.

Discussion

AML is a genetically heterogenous disease characterized by clonal expansion of immature myeloblasts associated with recurrent mutations including the cohesin complex [3–5,15,16,33]. Mutations in the subunits of the cohesin complex, *SMC1A, SMC3, RAD21*, and *STAG2*, have been found as early subclonal events in AML, although they are not observed in people with CHIP [5,15,16,18,19]. In contrast, *DNMT3A* mutations are among the most common initiating mutations in normal karyotype AML patients and the most frequently mutated genes in subjects with CHIP [3,34]. Cohesin mutations are mutually exclusive of one another and fall into two general categories: mutations in *RAD21* and *STAG2* are mainly truncations and frameshifts, whereas the majority of mutations in *SMC1A* and *SMC3* are missense. In AML, cohesin mutations are not associated with genomic instability, complex

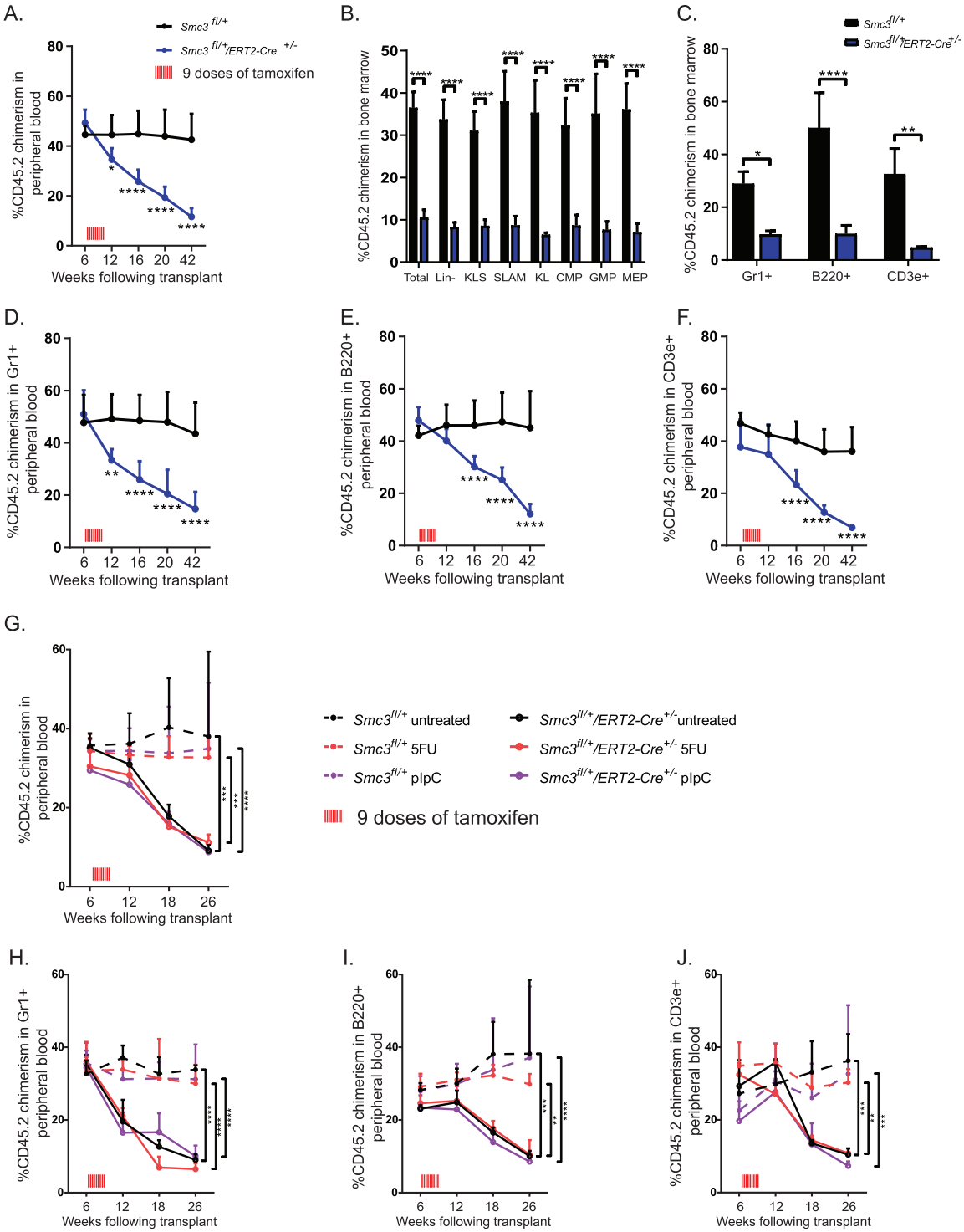

Figure 5. Competitive transplantation of *Smc3*-haploinsufficient BM cells. **(A–F)** Competitive repopulation assay using *Smc3*$^{fl/+}$*/ERT2-Cre*$^{+/-}$ BM cells and littermate *Smc3*$^{fl/+}$ BM cells with competitor CD45.1 × CD45.2 BM cells (three donor mice per group and 10 recipient mice per group). Following 6 weeks of engraftment, equal peripheral chimerism was validated and recipient mice were treated with nine doses of TAM. **(B,C)** Following 42 weeks, BM chimerism was analyzed ($n = 3$ mice per group). *Statistical significance by *t* test, *$p < 0.05$, **$p < 0.01$, ****$p < 0.0001$. **(D–F)** At interval time points during follow-up peripheral blood chimerism was evaluated within the Gr1, B220, and CD3e compartments. *Statistical significance by two-way ANOVA with Tukey's multiple-comparisons test, *$p < 0.05$, **$p < 0.01$, ****$p < 0.0001$. **(G–J)** Competitive repopulation assay of *Smc3*$^{fl/+}$*/ERT2-Cre*$^{+/-}$ BM cells under hematopoietic stresses ($n = 10$). As before, recipient mice were treated with nine doses of TAM after a 6-week engraftment. PIpC and 5-FU were given 16 weeks after transplantation, respectively. *Statistical significance by two-way ANOVA with Tukey's multiple-comparisons test, **$p < 0.01$, ***$p < 0.001$, ****$p < 0.0001$.

karyotypes, or monosomy karyotypes, suggesting alternative pathologic mechanisms [4,5,15].

To understand whether leukemia-associated *SMC3* missense mutations might have dominant-negative activities or phenocopy loss-of-function effects, we compared the consequences of *Smc3* deficiency and *Smc3* haploinsufficiency on murine hematopoiesis using conditionally deleted strategies. We began by validating the *Smc3* allele using whole-genome sequencing, RNA-Seq, and intracellular flow cytometry, which demonstrated correct integration, splicing of approximately 50% of alleles around exon 4 leading to a frameshift mutation and an early nonsense mutation, and reduced protein levels. Our findings suggest that leukemia-associated *SMC3* mutations are unlikely to have novel dominant-negative activities because homozygous *Smc3* deletion was incompatible with embryonic (Figure 2) or adult hematopoiesis (Figure 3). In these experiments, we observed the effects first in the myeloid compartment. However, because myeloid cells have a shorter half-life than other hematopoietic cell types, the augmented temporal phenotypes observed in these cell fractions may be influenced by greater turnover. Collectively, these studies demonstrate that *Smc3* is indispensable for embryonic and adult hematopoiesis and normal HSPC functions. Similar severe consequences for *Smc3* deficiency [35] and *Rad21* deficiency [36] have been observed, so cohesin genes appear to be essential in hematopoietic cells.

Leukemia-associated *SMC3* mutations are observed across all domains of the protein, and nearly one-third are nonsense or splice-site variants, suggesting that many of these mutations are likely to be associated with loss of function. Therefore, we investigated the effects of *Smc3* haploinsufficiency on murine hematopoiesis. Because these mutations are associated with leukemia, we predicted that *Smc3* haploinsufficiency would augment colony-forming capacity and provide hematopoietic cells a competitive advantage. However, we observed neither phenotype. Following *Smc3* haploinsufficiency induced with three different Cre models (*CMV-Cre, Vav1-Cre*, and *ERT2-Cre*), we observed normal CBCs, normal BM hematopoietic population distributions, and normal colony forming (Figures 4A–4E). We further examined expression signatures and ATAC-Seq under these steady-state conditions in $Smc3^{fl/+}/Vav1\text{-}Cre^{+/-}$ mice in which hematopoietic cells have consistently undergone heterozygous deletion and external perturbations are minimized; we observed little global dysregulation of gene expression or chromatin structure (Figures 4F and 4G). In both studies, internal markers (*Smc3* expression and peaks within the *Vav1* locus) served as controls and markers of the expected dynamic range.

In contrast, under conditions of chimeric competition, *Smc3* haploinsufficiency actually led to competitive disadvantage in vivo, with progressive population loss over time (Figures 5A–5F). In these studies, *Smc3* deletion was induced using *ERT2-Cre* following a period of 6 weeks after transplantation to facilitate engraftment and stem cell homeostasis prior to deletion. Under these conditions, activation of ERT2-Cre alone does not lead to stem cell toxicity and competitive disadvantage (Supplementary Figures E6A and E6B, online only, available at www.exphem.org), whereas activation of ERT2-Cre just prior to transplantation does [37]. Analysis of BM populations at the end of the study suggested reduction of populations with *Smc3* haploinsufficiency across progenitor and mature cell types, eliminating the possibility that *Smc3* haploinsufficiency led to a profound maturation block that prevented leukocyte peripheralization. The competitive disadvantage induced by somatic *Smc3* acquisition was unexpected; therefore, we determined whether specific forms of hematopoietic stress might enable a competitive advantage that could facilitate stem cell expansion and ultimately enable leukemogenesis. We again observed a competitive disadvantage that persisted following a stem cell stressor (5-FU exposure) and an inflammatory stressor (pIpC exposure) (Figure 5G-J). Finally, because *SMC3* mutations may not be the first acquired mutation during leukemogenic chronicity, we investigated whether *Dnmt3a* haploinsufficiency might facilitate *Smc3* phenotypes. Germline *Dnmt3a* haploinsufficiency partially abrogated the myeloid competitive disadvantage of somatically acquired *Smc3* haploinsufficiency (Figure 6), suggesting that *SMC3* mutations may require preexisting cooperating mutations to facilitate their action. Additionally, these studies do not eliminate the possibility that the frequently observed *SMC3* missense mutations may possess novel gain-of-function activity not accessed in these *Smc3*-haploinsufficient studies.

Therefore, under conditions of homeostasis, where all hematopoietic cells have *Smc3* haploinsufficiency, murine *Smc3* haploinsufficiency does not appear to grossly dysregulate hematopoietic feedback mechanisms or alter normal hematopoietic maturation or self-renewal ex vivo. However, under conditions of competitive transplantation, we observed a disadvantage in hematopoietic cells across both myeloid and lymphoid lineages, suggesting reduced cell production at a multipotent progenitor level.

These results contrast with previously published work using either knock-down strategies in $CD34^+$ cord blood cells or using Mx1-Cre activation with pIpC. Specifically, knocking down of *Smc3* using shRNA or *RAD21* and *SMC1A* mutants have been shown to increase self-renewal in human cord blood $CD34^+$ HSPCs ex vivo [38,39]. *Smc3* haploinsufficiency induced by Mx1-Cre exhibited shifts in hematopoietic cell populations, colony forming, and competitive transplantation advantage when deleted using Mx1-Cre 2 weeks after transplantation [35].

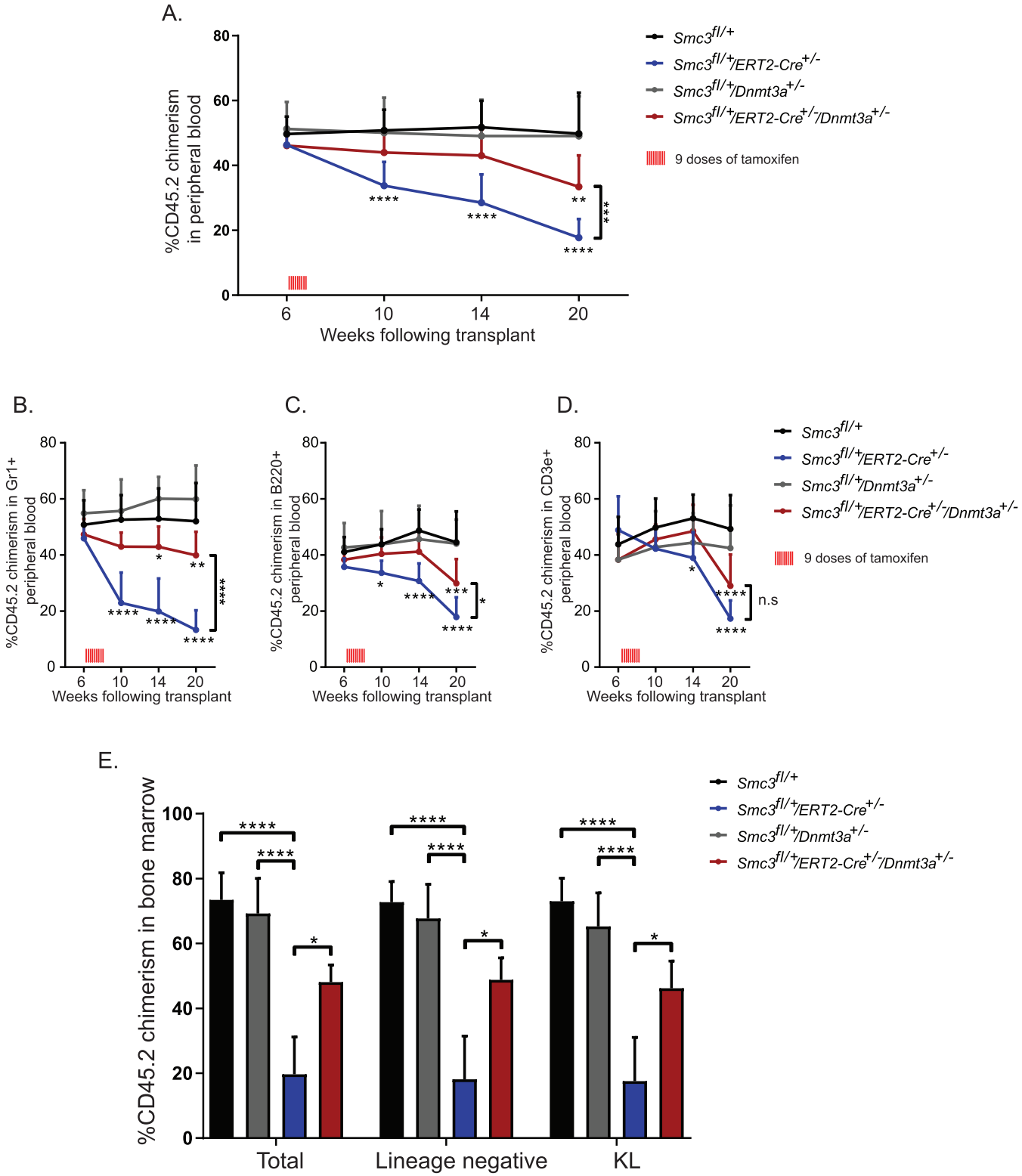

Figure 6. Effect of *Dnmt3a* haploinsufficiency on competitive disadvantage in *Smc3* haploinsufficient BM cells. **(A–D)** Competitive repopulation assay of *Smc3*$^{fl/+}$/*ERT2-Cre*$^{+/-}$/*Dnmt3a*$^{+/-}$ BM cells and indicated littermate controls ($n = 10$ mice per group). As in Figure 5, total BM cells were allowed to engraft for 6 weeks and equivalent chimerism was validated before treatment of all cohorts with nine doses of TAM (3 mg/day). Peripheral blood chimerism was evaluated by flow cytometry at the indicated time points. **(E)** BM chimerism assessed by flow cytometry 26 weeks after engraftment ($n = 4$ mice in each group). *Statistical significance by two-way ANOVA with Tukey's multiple-comparisons test, *$p < 0.05$, **$p < 0.01$, ***$p < 0.001$, ****$p < 0.0001$.

These data suggest that differences in the models may interact with the biological consequences of *Smc3* reduction through as-yet undefined mechanisms.

In addition, It is worth noting that other MDS- or AML-associated mutations such as *U2AF1* [40,41], *SRSF2* [42,43], *SF3B1* [44–48], and *ASXL1* [49,50] are associated with having a competitive disadvantage, which may seem counterintuitive for recurring leukemia mutations observed in patients, but appears to be recurrent biology.

The observed defects in hematopoietic cells with *Smc3* deficiency and haploinsufficiency may reflect population data from the ExAC database, where germline cohesin mutations are observed at lower than expected frequencies, suggesting a significant disadvantage in population fitness. No loss-of-function variants are detected in *SMC3, SMC1A, STAG2*, or *RAD21* (based on statistical models of case numbers and gene size, the expected numbers of loss-of-function variants were 58.5, 32, 42.7, and 21.8, respectively). Missense variants were also significantly underrepresented in *SMC3, SMC1A*, and *STAG2*, but not in *RAD21* ($z = 6.25$, 6.59, 5.11, and 2.76, respectively; more positive scores indicate fewer variants observed than expected). Of the published AML-associated missense mutations, only one is reported in ExAC (K795E occurring in 3/121,384 alleles), although synonymous changes (R155R, Q367Q, and R391R) and alternative amino acid changes (N604S and I1001L) are noted [51].

In recent decades, mutations in cohesin complex genes have been associated with genetic syndromes referred to as cohesinopathies. Several important features differ between cohesinopathies and AML-associated cohesin mutations. Mutations associated with cohesinopathy tend to be in cohesin adapter proteins such as *NILS, HDAC8*, and *ESCO2*, with fewer mutations observed in *SMC3, SMC1A, RAD21*, or *STAG2* [52]. Cohesinopathies are associated with facial dysmorphism, cognitive impairment, prenatal and postnatal growth delay, and multiorgan involvement and the clinical manifestations appear milder in cases with *SMC3* and *SMC1A* mutations compared with *NIPBL* mutations [53]. Hematopoietic alterations have not been reported with cohesinopathy, nor has the development of AML. Likewise, the accumulation of aneuploidies and others chromosomal aberrations has been a recurrent feature of cohesinopathy, whereas this phenotype is largely absent in cohesin-mutated AML cases, which typically present with normal karyotypes. Intriguingly, copy number gains of *STAG2* or *SMC1A* also have been associated with cohesinopathy phenotypes [54–56], suggesting that there may be a critical window of adequate cohesin activity and that alterations in either direction may be detrimental. In contrast to these human data, in our mouse model, germline heterozygous *Smc3* deletion was tolerated using X-linked *CMV-Cre*, which is expressed during early embryogenesis. The heterozygous $Smc3^{+/-}$/*CMV-Cre*$^{+/-}$ female progenies had no obvious developmental defects and had normal hematopoietic homeostasis in the BM (Supplementary Figure E4, online only, available at www.exphem.org). The normal hematopoietic cell numbers and differentials in the mice reflect the maintained hematopoiesis of cohesinopathies, whereas the normal number of *Smc3*-haploinsufficient pups contrasts with the near absence of cohesin mutations in the human population data. This discrepancy may be due to differences between mouse and human biology; alternatively, cohesinopathy mutations may be associated with gain-of-function activity not recapitulated with this allele or activity not related directly to the SMC1A/SMC3 complex.

In summary, we did not observe evidence of impaired differentiation or augmented self-renewal ex vivo or in vivo when *Smc3* haploinsufficiency was generated using *CMV-Cre, Vav1-Cre, and ERT2-Cre*. Instead, *Smc3* haploinsufficiency was associated with a competitive disadvantage, with an early bias towards phenotypes in the myeloid compartment. In AML patients, *SMC3* mutations are typically early, but not initiating, genetic events. These data also suggest that preexisting mutations may be required to enable leukemogenic consequences of *SMC3* mutagenesis and to permit productive clonal expansion. Future studies are needed to determine the combination of cooperating mutations that predispose HSPCs to *SMC3*-induced leukemic transformation and clonal dominance.

Acknowledgments

This work was supported by a V Foundation Scholar award (JSW) and the National Cancer Institute (AML-SPORE P50 CA171963). We thank Deborah Laflamme and Conner York for excellent animal husbandry support, Nicole Helton for technical assistance with library construction, David Spencer for providing assistance with ATAC-Seq analysis, and Timothy J. Ley and Grant A. Challen for critically reading the manuscript.

Author contributions

TW and JSW designed experiments, performed experiments, interpreted data, and wrote the paper. BG, GH, CAM, and ODM performed experiments and interpreted data.

Conflict interest disclosure

The authors declare no competing financial interests.

References

1. Saultz JN, Garzon R. Acute myeloid leukemia: a concise review. J Clin Med. 2016;5:E33.
2. Lagunas-Rangel FA, Chávez-Valencia V, Gómez-Guijosa MÁ, Cortes-Penagos C. Acute myeloid leukemia: genetic alterations and their clinical prognosis. Int J Hematol Oncol Stem Cell Res. 2017;11:328–339.

3. Cancer Genome Atlas Research Network, Ley TJ, Miller C, Ding L, et al. Genomic and epigenomic landscapes of adult de novo acute myeloid leukemia. N Engl J Med. 2013;368:2059–2074.
4. Kon A, Shih LY, Minamino M, et al. Recurrent mutations in multiple components of the cohesin complex in myeloid neoplasms. Nat Genet. 2013;45:1232–1237.
5. Thota S, Viny AD, Makishima H, et al. Genetic alterations of the cohesin complex genes in myeloid malignancies. Blood. 2014;124:1790–1798.
6. Yoshida K, Toki T, Okuno Y, et al. The landscape of somatic mutations in Down syndrome-related myeloid disorders. Nat Genet. 2013;45:1293–1299.
7. Barber TD, McManus K, Yuen KWY, et al. Chromatid cohesion defects may underlie chromosome instability in human colorectal cancers. Proc Natl Acad Sci. 2008;105:3443–3448.
8. Gorringe KL, Ramakrishna M, Williams LH, et al. Are there any more ovarian tumor suppressor genes? A new perspective using ultra high-resolution copy number and loss of heterozygosity analysis. Genes Chromosomes Cancer. 2009;48:931–942.
9. Bailey ML, O'Neil NJ, van Pel DM, Solomon DA, Waldman T, Hieter P. Glioblastoma cells containing mutations in the cohesin component STAG2 are sensitive to PARP inhibition. Mol Cancer Ther. 2014;13:724–732.
10. Solomon DA, Kim J-S, Bondaruk J, et al. Frequent truncating mutations of STAG2 in bladder cancer. Nat Genet. 2013;45:1428–1430.
11. Balbás-Martínez C, Sagrera A, Carrillo-de-Santa-Pau E, et al. Recurrent inactivation of STAG2 in bladder cancer is not associated with aneuploidy. Nat Genet. 2013;45:1464–1469.
12. Solomon DA, Kim T, Diaz-Martinez LA, et al. Mutational inactivation of STAG2 causes aneuploidy in human cancer. Science. 2011;333:1039–1043.
13. Remeseiro S, Cuadrado A, Gómez-López G, Pisano DG, Losada A. A unique role of cohesin-SA1 in gene regulation and development. EMBO J. 2012;31:2090–2102.
14. Mannini L, Cucco F, Quarantotti V, Krantz ID, Musio A. Mutation spectrum and genotype-phenotype correlation in Cornelia de Lange syndrome. Hum Mutat. 2013;34:1589–1596.
15. Welch JS, Ley TJ, Link DC, et al. The origin and evolution of mutations in acute myeloid leukemia. Cell. 2012;150:264–278.
16. Thol F, Bollin R, Gehlhaar M, et al. Mutations in the cohesin complex in acute myeloid leukemia: clinical and prognostic implications. Blood. 2014;123:914–920.
17. Conese M, Liso A. Cohesin complex is a major player on the stage of leukemogenesis. Stem Cell Investig. 2016;3:18.
18. Xie M, Lu C, Wang J, et al. Age-related mutations associated with clonal hematopoietic expansion and malignancies. Nat Med. 2014;20:1472–1478.
19. Jaiswal S, Natarajan P, Silver AJ, et al. Clonal hematopoiesis and risk of atherosclerotic cardiovascular disease. N Engl J Med. 2017;377:111–121.
20. Cole CB, Russler-Germain DA, Ketkar S, et al. Haploinsufficiency for DNA methyltransferase 3A predisposes hematopoietic cells to myeloid malignancies. J Clin Invest. 2017;127:3657–3674.
21. Ball AR, Chen YY, Yokomori K. Mechanisms of cohesin-mediated gene regulation and lessons learned from cohesinopathies. Biochim Biophys Acta. 2014;1839:191–202.
22. Wendt KS, Yoshida K, Itoh T, et al. Cohesin mediates transcriptional insulation by CCCTC-binding factor. Nature. 2008;451:796–801.
23. Merkenschlager M, Odom DT. CTCF and cohesin: linking gene regulatory elements with their targets. Cell. 2013;152:1285–1297.
24. Schmidt D, Schwalie PC, Ross-Innes CS, et al. A CTCF-independent role for cohesin in tissue-specific transcription. Genome Res. 2010;20:578–588.
25. Trapnell C, Roberts A, Goff L, et al. Differential gene and transcript expression analysis of RNA-seq experiments with TopHat and Cufflinks. Nat Protoc. 2012;7:562–578.
26. Buenrostro JD, Giresi PG, Zaba LC, Chang HY, Greenleaf WJ. Transposition of native chromatin for fast and sensitive epigenomic profiling of open chromatin, DNA-binding proteins and nucleosome position. Nat Methods. 2013;10:1213–1218.
27. Zhang Y, Liu T, Meyer CA, et al. Model-based analysis of ChIP-Seq (MACS). Genome Biol. 2008;9:R137.
28. Quinlan AR, Hall IM. BEDTools: a flexible suite of utilities for comparing genomic features. Bioinforma Oxf Engl. 2010;26:841–842.
29. Ramírez F, Dündar F, Diehl S, Grüning BA, Manke T. deepTools: a flexible platform for exploring deep-sequencing data. Nucleic Acids Res. 2014;42(Web Server issue):W187–W191.
30. Love MI, Huber W, Anders S. Moderated estimation of fold change and dispersion for RNA-seq data with DESeq2. Genome Biol. 2014;15:550.
31. Tusher VG, Tibshirani R, Chu G. Significance analysis of microarrays applied to the ionizing radiation response. Proc Natl Acad Sci U S A. 2001;98:5116–5121.
32. Kanehisa M, Sato Y, Kawashima M, Furumichi M, Tanabe M. KEGG as a reference resource for gene and protein annotation. Nucleic Acids Res. 2016;44:D45–D462.
33. Walter MJ, Shen D, Ding L, et al. Clonal architecture of secondary acute myeloid leukemia. N Engl J Med. 2012;366:1090–1098.
34. Genovese G, Kähler AK, Handsaker RE, et al. Clonal hematopoiesis and blood-cancer risk inferred from blood DNA sequence. N Engl J Med. 2014;371:2477–2487.
35. Viny AD, Ott CJ, Spitzer B, et al. Dose-dependent role of the cohesin complex in normal and malignant hematopoiesis. J Exp Med. 2015;212:1819–1832.
36. Xu H, Balakrishnan K, Malaterre J, et al. Rad21-cohesin haploinsufficiency impedes DNA repair and enhances gastrointestinal radiosensitivity in mice. PloS One. 2010;5:e12112.
37. Welch JS, Yuan W, Ley TJ. PML-RARA can increase hematopoietic self-renewal without causing a myeloproliferative disease in mice. J Clin Invest. 2011;121:1636–1645.
38. Mullenders J, Aranda-Orgilles B, Lhoumaud P, et al. Cohesin loss alters adult hematopoietic stem cell homeostasis, leading to myeloproliferative neoplasms. J Exp Med. 2015;212:1833–1850.
39. Mazumdar C, Shen Y, Xavy S, et al. Leukemia-associated cohesin mutants dominantly enforce stem cell programs and impair human hematopoietic progenitor differentiation. Cell Stem Cell. 2015;17:675–688.
40. Shirai CL, Ley JN, White BS, et al. Mutant U2AF1 expression alters hematopoiesis and pre-mRNA splicing in vivo. Cancer Cell. 2015;27:631–643.
41. Fei DL, Zhen T, Durham B, et al. Impaired hematopoiesis and leukemia development in mice with a conditional knock-in allele of a mutant splicing factor gene U2af1. Proc Natl Acad Sci U S A. 2018;115:E10437–E10446.
42. Kim E, Ilagan JO, Liang Y, et al. SRSF2 mutations contribute to myelodysplasia by mutant-specific effects on exon recognition. Cancer Cell. 2015;27:617–630.
43. Komeno Y, Huang Y-J, Qiu J, et al. SRSF2 is essential for hematopoiesis, and its myelodysplastic syndrome-related mutations dysregulate alternative pre-mRNA splicing. Mol Cell Biol. 2015;35:3071–3082.

44. Wang C, Sashida G, Saraya A, et al. Depletion of Sf3b1 impairs proliferative capacity of hematopoietic stem cells but is not sufficient to induce myelodysplasia. Blood. 2014;123:3336–3343.
45. Matsunawa M, Yamamoto R, Sanada M, et al. Haploinsufficiency of Sf3b1 leads to compromised stem cell function but not to myelodysplasia. Leukemia. 2014;28:1844–1850.
46. Visconte V, Tabarroki A, Zhang L, et al. Splicing factor 3b subunit 1 (Sf3b1) haploinsufficient mice display features of low risk myelodysplastic syndromes with ring sideroblasts. J Hematol Oncol. 2014;7:89.
47. Obeng EA, Chappell RJ, Seiler M, et al. Physiologic expression of Sf3b1(K700E) causes impaired erythropoiesis, aberrant splicing, and sensitivity to therapeutic spliceosome modulation. Cancer Cell. 2016;30:404–417.
48. Mupo A, Seiler M, Sathiaseelan V, et al. Hemopoietic-specific Sf3b1-K700E knock-in mice display the splicing defect seen in human MDS but develop anemia without ring sideroblasts. Leukemia. 2017;31:720–727.
49. Abdel-Wahab O, Gao J, Adli M, et al. Deletion of Asxl1 results in myelodysplasia and severe developmental defects in vivo. J Exp Med. 2013;210:2641–2659.
50. Nagase R, Inoue D, Pastore A, et al. Expression of mutant Asxl1 perturbs hematopoiesis and promotes susceptibility to leukemic transformation. J Exp Med. 2018;215:1729–1747.
51. ExAC Browser. Available from: http://exac.broadinstitute.org/gene/ENSG00000108055. Accessed 18 May 2018.
52. Cucco F, Musio A. Genome stability: What we have learned from cohesinopathies. Am J Med Genet C Semin Med Genet. 2016;172:171–178.
53. Ramos FJ, Puisac B, Baquero-Montoya C, et al. Clinical utility gene card for: Cornelia de Lange syndrome. Eur J Hum Genet. 2015;23.
54. Kumar R, Corbett MA, Van Bon BW, et al. Increased STAG2 dosage defines a novel cohesinopathy with intellectual disability and behavioral problems. Hum Mol Genet. 2015;24:7171–7181.
55. Leroy C, Jacquemont ML, Doray B, et al. Xq25 duplication: the crucial role of the STAG2 gene in this novel human cohesinopathy. Clin Genet. 2016;89:68–73.
56. Baquero-Montoya C, Gil-Rodríguez MC, Teresa-Rodrigo ME, et al. Could a patient with SMC1A duplication be classified as a human cohesinopathy? Clin Genet. 2014;85:446–451.

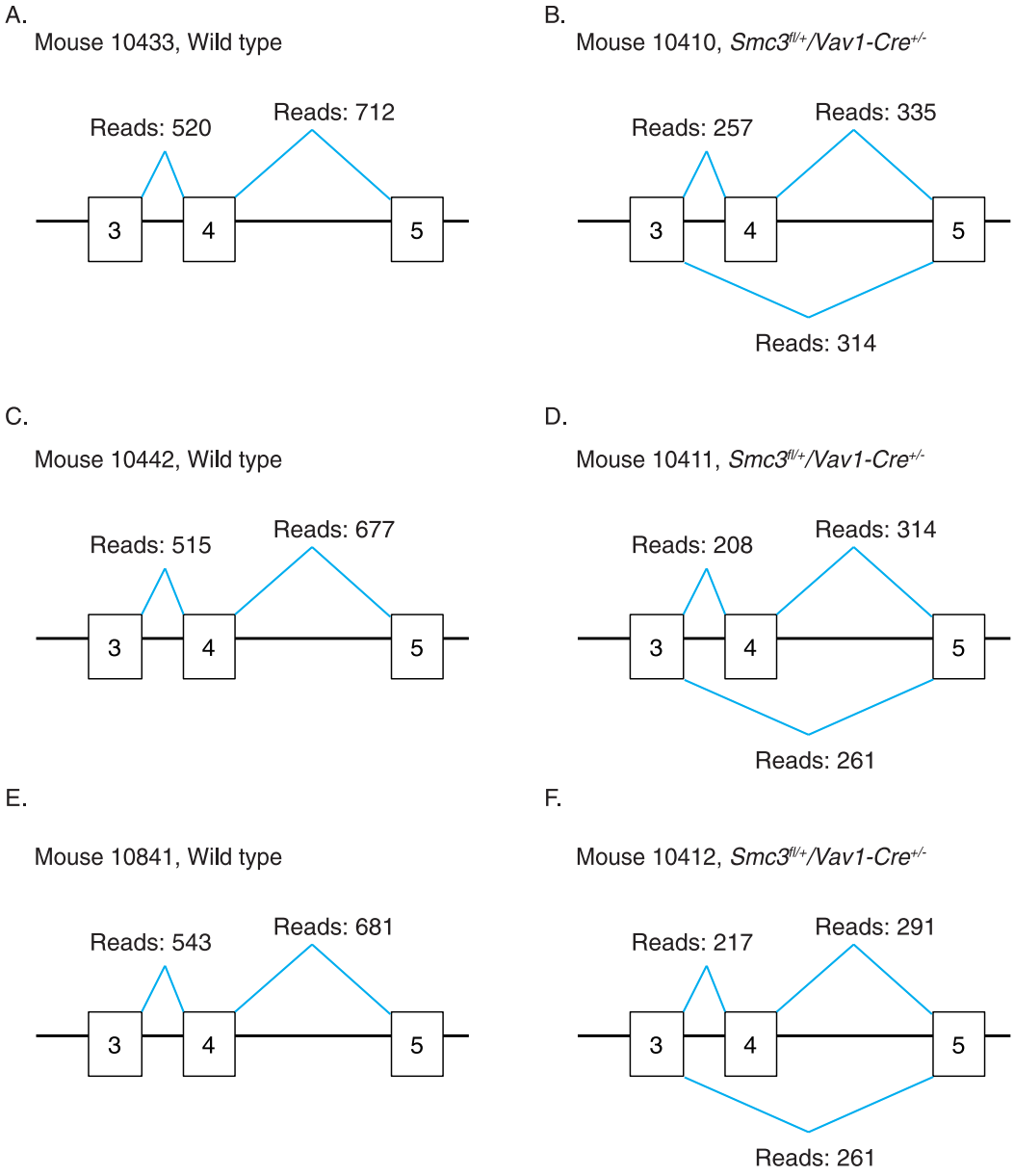

Figure E1. Splicing analysis of exon 3 to exon 5 in wild-type and *Smc3*$^{fl/+}$*/Vav1-Cre*$^{+/-}$ KL cells. Lin-cKit+Sca1- bone marrow cells were subjected to RNA-Seq (Figure 1C and 4F). Schema indicates total number of reads spanning each splice junction from indicated mice.

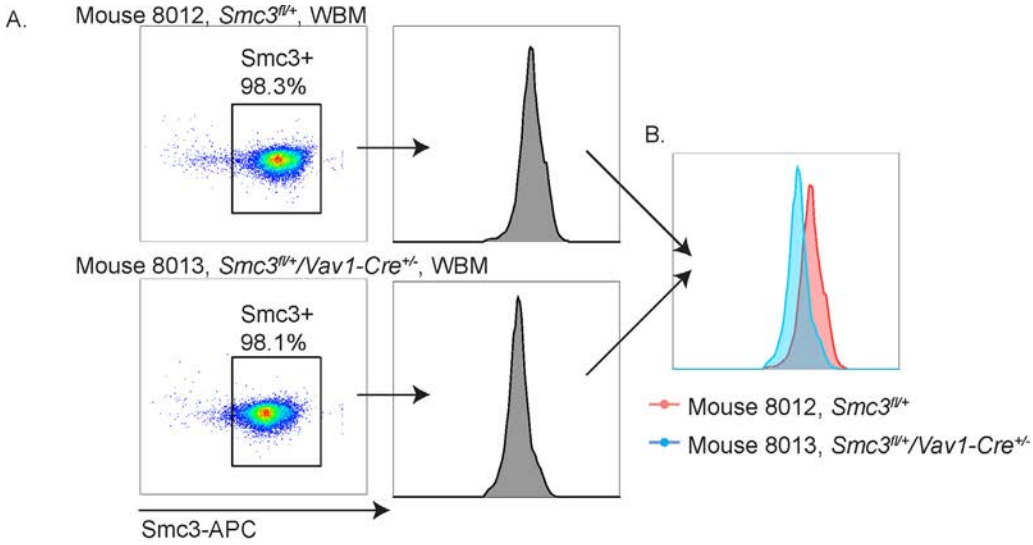

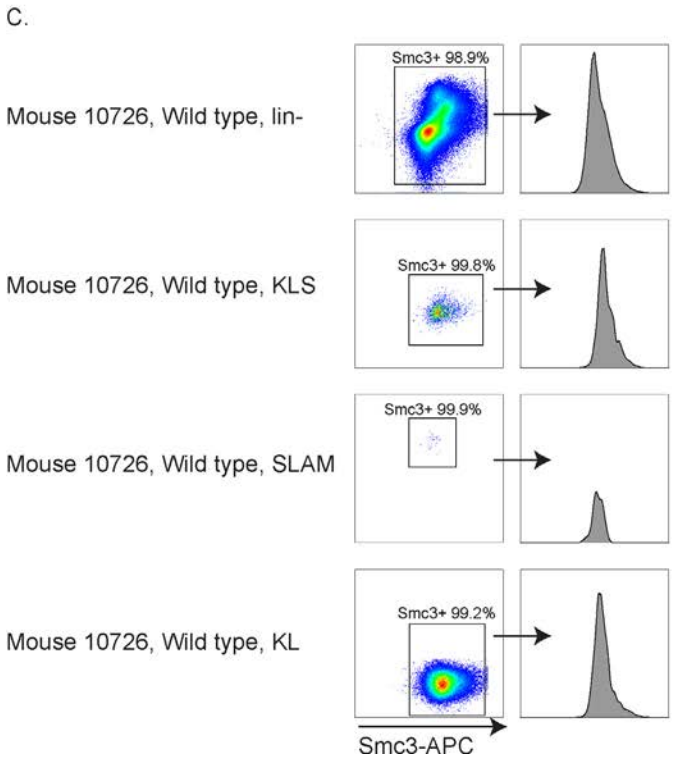

Figure E2. Representative plot of intracellular flow cytometry data (Figure 1D-E). (A) Percentages of Smc3+ cells (left) and mean fluorescence intensity (MFI) (right) of WBM from mice used in Figure 1D. (B). Overlay of the two MFI plots. (C) Percentages of Smc3+ cells (left) and mean fluorescence intensity (MFI) (right) of lin-, KLS, SLAM, and KL cells from mouse used in Figure 1E. The height of the peak is proportional to the number of events collected.

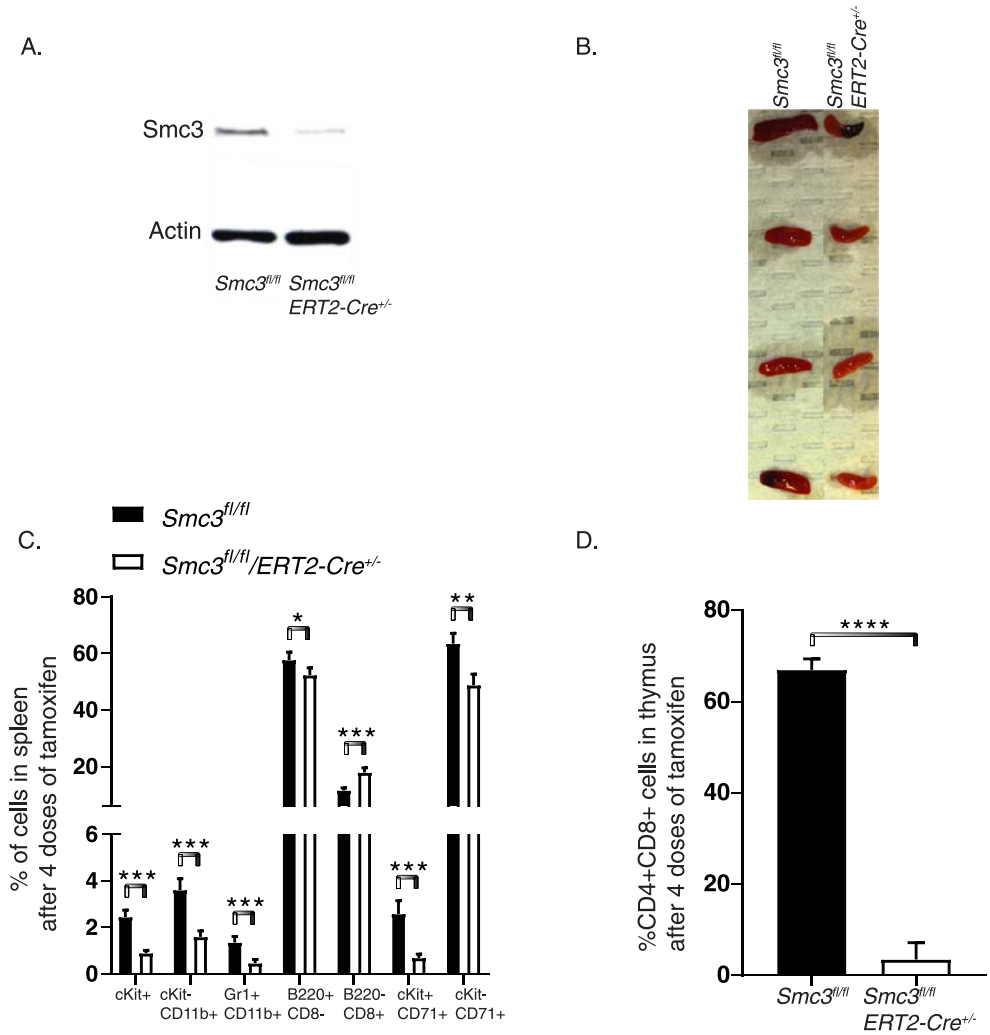

Figure E3. Analysis of homozygous somatic Smc3 deletion (A) Western blot of Smc3 in total bone marrow cells following 4 doses of tamoxifen in indicated mice. (B) Image of spleens from *Smc3$^{fl/+}$/ERT2-Cre$^{+/-}$* and *Smc3$^{fl/+}$* littermate controls following 4 doses of tamoxifen. (C-D) Proportion of bone marrow cells and thymocytes with indicated immunophenotypes following 4 doses of tamoxifen in *Smc3$^{fl/+}$/ERT2-Cre$^{+/-}$* mice and littermate controls (n = 4 mice per group), *Denotes statistical significance by t test, *$p < 0.05$, **$p < 0.01$, ***$p < 0.001$, ****$p < 0.0001$.

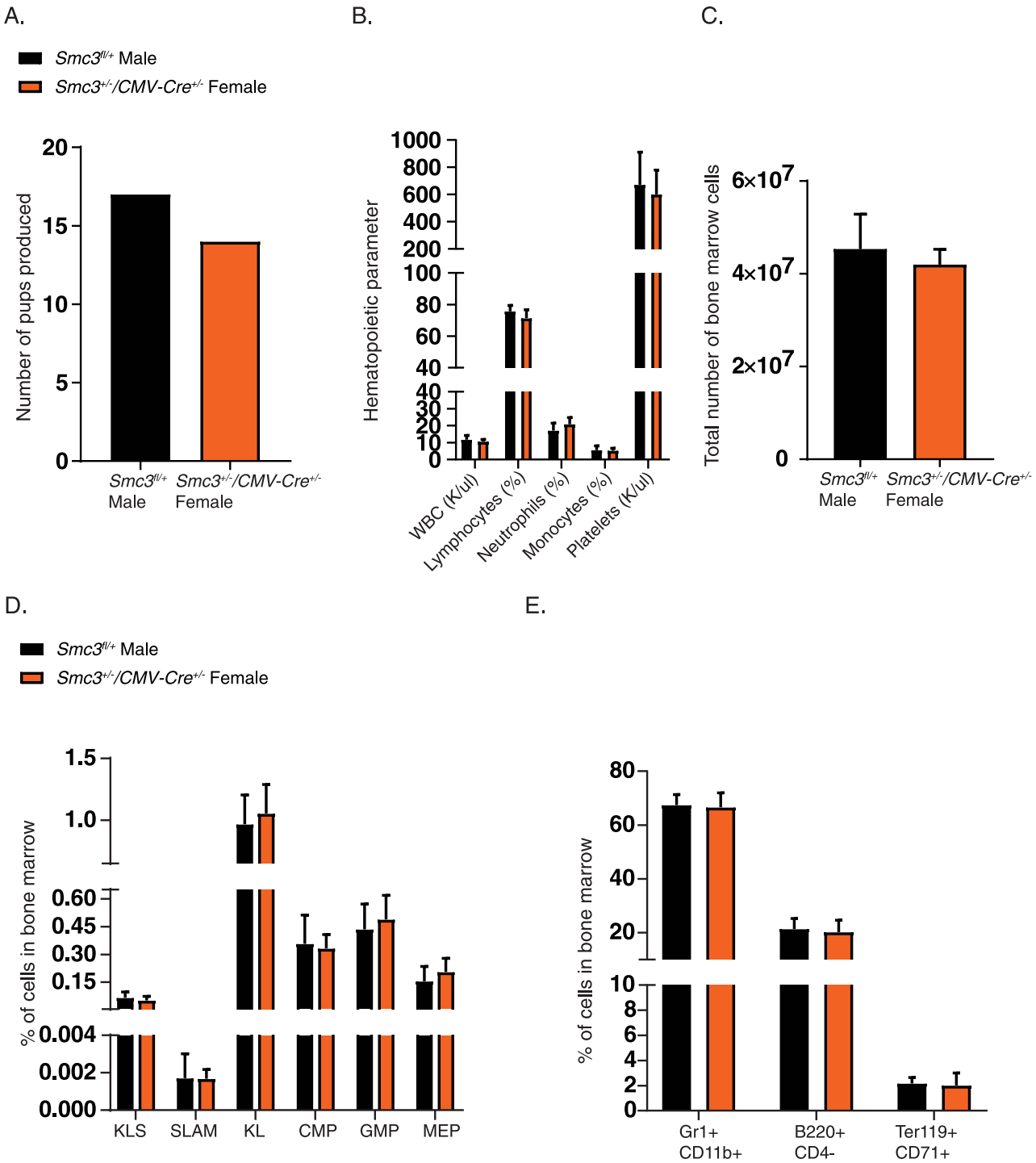

Figure E4. Analysis of germline heterozygous *Smc3* deletion. (A) Numbers of male vs. female pups generated from $Smc3^{fl/fl}$ and $CMV\text{-}Cre^{+/-}$ intercrosses (of note, CMV-Cre is X-linked). (B-E) Complete blood counts, total number of bone marrow cells, percentages of HSPCs, and cells of myeloid (Gr1+ CD11b+), B cells (B220+ CD4-), and erythroid cells (Ter119+ CD71+) in $Smc3^{+/-}/CMV\text{-}Cre^{+/-}$ females and $Smc3^{fl/+}$ littermate males, (n = 4 mice per group).

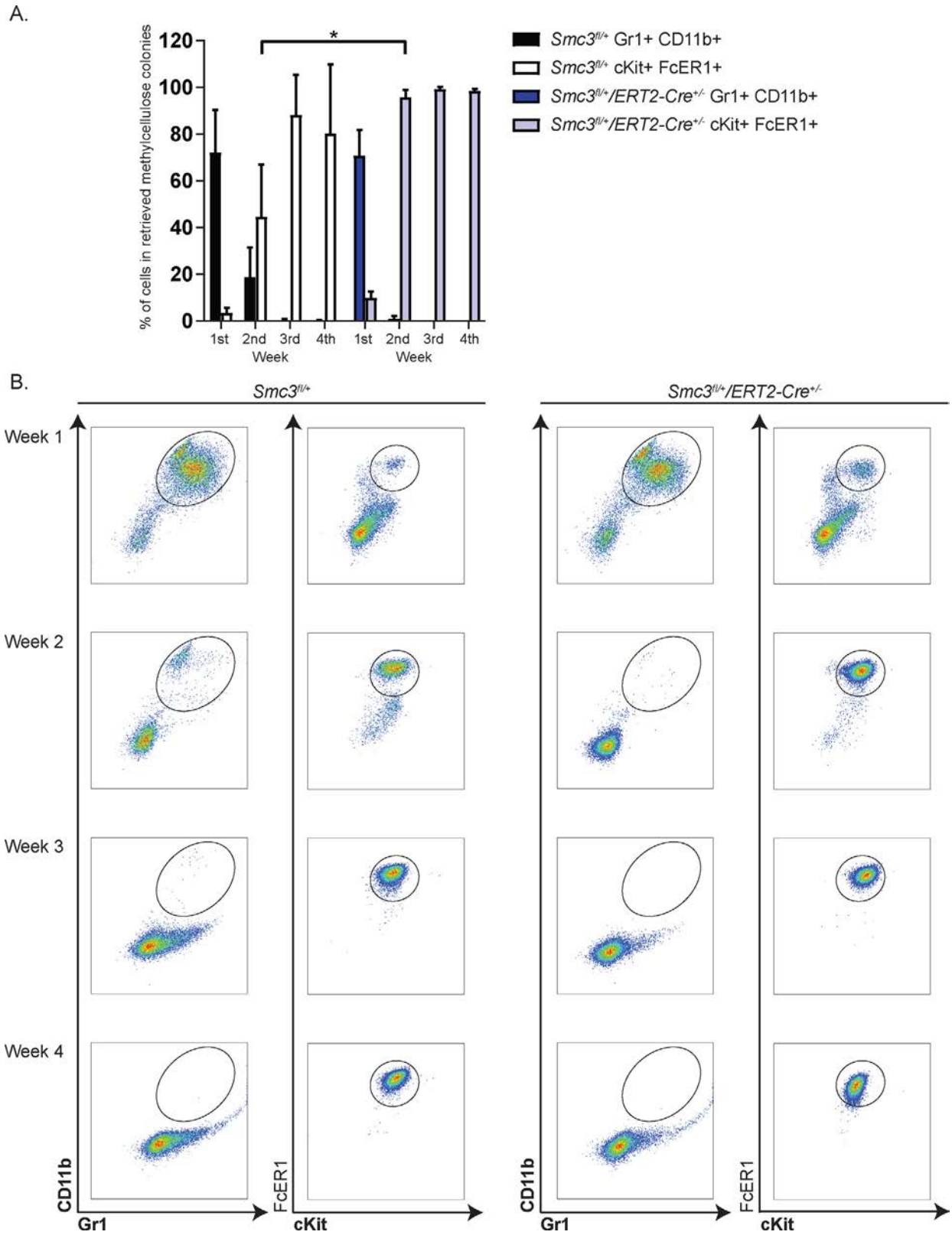

Figure E5. Immunophenotypic analysis of colonies in serial replating assay ex vivo (Figure 4C-E). (A) Percentages of Gr1+ CD11b+ and cKit+ FcER1+ cells in the *Smc3*$^{fl/+}$ and *Smc3*$^{fl/+}$*/ERT2-Cre*$^{+/-}$ colonies week 1-4 respectively (n = 4 mice per group). (B) Representative plot of the *Smc3*$^{fl/+}$ and *Smc3*$^{fl/+}$*/ERT2-Cre*$^{+/-}$ colonies week 1-4. *Denotes statistical significance by t test, *$p < 0.05$.

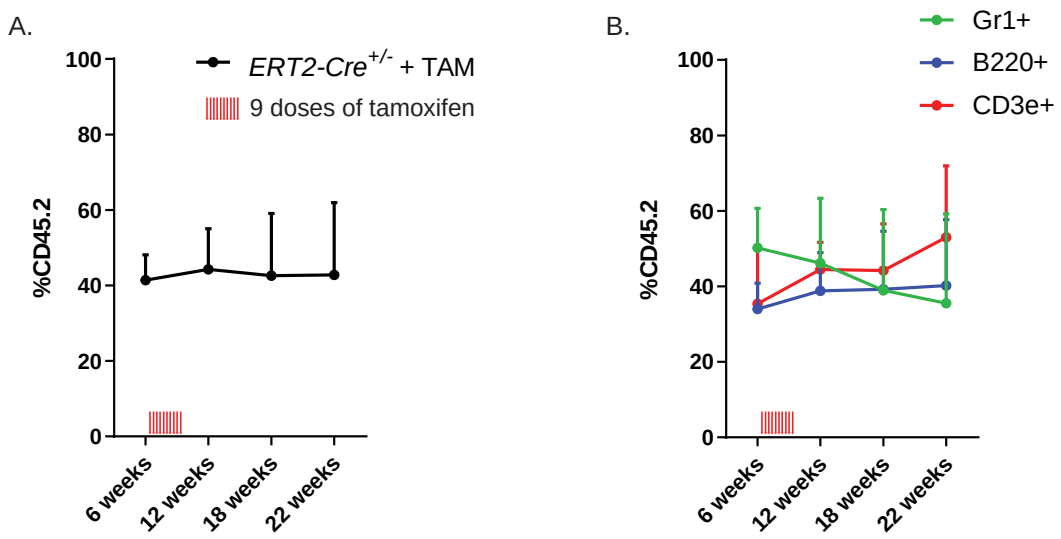

Figure E6. Competitive transplantation of *ERT2-Cre*$^{+/-}$ bone marrow cells (A) Competitive repopulation assay using *ERT2-Cre*$^{+/-}$ BM cells with competitor CD45.1 x CD45.2 bone marrow cells (3 donor mice and 5 recipient mice). Following 6 weeks of engraftment, equal peripheral chimerism was validated and recipient mice were treated with 9 doses of tamoxifen. (B) At interval time-points during follow-up peripheral blood chimerism was evaluated within the Gr1, B220, and CD3e compartments.